Antiferromagnetic structure of exchange-coupled La_{0.7}Sr_{0.3}FeO_{3} thin films studied using angle-dependent x-ray absorption spectroscopy

Yue Jia, Rajesh V. Chopdekar, Padraic Shafer, Elke Arenholz, Zhiqi Liu, Michael D. Biegalski, and Yayoi Takamura

Phys. Rev. B **96**, 214411 — Published 8 December 2017

DOI: 10.1103/PhysRevB.96.214411

Antiferromagnetic structure of exchange coupled $La_{0.7}Sr_{0.3}FeO_3$ thin films studied using angle-dependent x-ray absorption spectroscopy

Yue Jia[1], Rajesh V. Chopdekar[1], Padraic Shafer[2], Elke Arenholz[2], Zhiqi Liu[3,+], Michael D. Biegalski[3], and Yayoi Takamura[1,*]

[1]*Department of Materials Science Engineering, University of California, Davis, Davis, California, 95616, USA*

[2]*Advanced Light Source, Lawrence Berkeley National Laboratory, Berkeley, California, 94720, USA*

[3]*Center for Nanophase Materials Sciences, Oak Ridge National Laboratory, Oak Ridge, Tennessee, 37831, USA*

Abstract

The magnetic structure of exchange coupled antiferromagnetic (AF) layers in epitaxial $La_{0.7}Sr_{0.3}MnO_3$ (LSMO)/$La_{0.7}Sr_{0.3}FeO_3$ (LSFO) superlattices grown on (111)-oriented $SrTiO_3$ substrates was studied using angle-dependent x-ray absorption spectroscopy utilizing linearly polarized x-rays. We demonstrate the development of the measurement protocols needed to determine the orientation of the LSFO antiferromagnetic (AF) spin axis and how it responds to an applied magnetic field due to exchange interactions with an adjacent ferromagnetic layer. A small energy difference exists between two types of AF order: the majority of the AF moments cant out-of-the-plane of the film along the $< 110 >$ or $< 100 >$ directions depending on the LSFO layer thickness. In response to an applied magnetic field, these canted moments are aligned with a single $< 110 >$ or $< 100 >$ direction that maintains a nearly perpendicular orientation relative to the LSMO sublayer magnetization. The remaining AF moments lie within the (111)-plane and these in-plane moments can be reoriented to an arbitrary in-plane direction to lie parallel to the LSMO sublayer magnetization. These results demonstrate that the magnetic order of AF thin films and heterostructures is far more complex than in bulk LSFO and can be tuned with orientation, thickness, and applied magnetic field.

[+]Current institution: School of Materials Science and Engineering, Beihang University, Beijing 100191, China

*Corresponding author: ytakamura@ucdavis.edu

Introduction

Perovskite oxides display a wide spectrum of magnetic properties and with recent advances in thin film deposition techniques, it is possible to synthesize epitaxial thin film heterostructures consisting of alternating layers with different magnetic orders.[1] The majority of research on perovskite oxide heterostructures has been limited to the (001)-orientation, primarily due to the difficulty to obtain smooth interfaces on other orientations where different growth mechanisms dominate.[2] In contrast, (111)-oriented perovskite oxide heterostructures possess a buckled honeycomb lattice resembling graphene and are composed of alternating, highly polar layers. These structural differences lead to intriguing properties absent in their (001)-oriented counterparts as reported in recent theoretical and experimental work.[3, 4]

Exchange coupling between adjacent ferromagnetic (FM) and antiferromagnetic (AF) layers has been of interest for fundamental and applied research during the last several decades.[5] Successful applications include giant magnetoresistive heads in hard disk drives which use exchange bias to pin the direction of a reference FM layer. Exchange coupling along with magneto-electric coupling between ferroelectric and AF orders in multiferroic materials such as $BiFeO_3$, offers a new pathway to electrical control of magnetism.[6] A key aspect in the research of exchange coupling between perovskite oxides is to understand the magnetic structure of the AF layer and to probe how it can be modified by interfacial effects including charge transfer, orbital reconstruction, and strain.[7] Ultimately, it is this interface magnetic structure of the AF material that determines the nature of the exchange coupling in perovskite oxide heterostructures. With uncompensated spins at the interface, *exchange bias* can occur, where the magnetic moments of the FM material tend to align parallel to the AF spins at the interface to reduce the exchange energy.[8] Alternatively, interfaces with compensated AF spins experience spin frustration where the moments of the FM layer align perpendicular to the AF spin axis in order to minimize energy. This type of coupling is referred to as *spin-flop coupling* and is characterized by the ability of the AF spins to be reoriented by a moderate external magnetic field through the coupling with the FM layer.[5, 9, 10] Due to the limited volume of the AF layers in FM/AF thin film heterostructures, neutron diffraction is usually not a feasible option to characterize the AF magnetic structure. As an alternative, indirect probes such as the shape of hysteresis loops have been used to infer the AF structure, [11, 12] however this approach is limited by the fact that hysteresis loops are often dominated by the signal from the FM layers.

In contrast, soft x-ray magnetic linear dichroism (XMLD) is a powerful tool to directly probe the AF properties in thin films. The angular dependence of the XMLD signal, in which the measurements are performed at a series of different geometries, can reveal a wealth of information about the AF order. Previous angle-dependent XMLD studies have investigated effects such as the impact of field cooling on the AF structure of polycrystalline NiO films,[13] crystal field symmetry of Fe_3O_4 thin films,[14] exchange coupling at Co/NiO (001) interfaces,[15] and population of rotatable AF spins at the CoO/Fe interface.[16] In general, XMLD signals are sensitive to crystal field effects, orbital ordering, and the charge distribution around the AF moments.[17, 18] Therefore, careful design of the experimental geometry is needed to identify whether the observed dichroism is due to the AF spin order and/or of non-magnetic origin. In this work, we demonstrate the development of the measurement protocols needed to measure and interpret the angular dependence of the

absorption spectrum of linearly polarized x-rays from (111)-oriented heterostructures with 3-fold in-plane rotational symmetry. These measurement are used to elucidate the AF structure in superlattices consisting of alternating layers of FM $La_{0.7}Sr_{0.3}MnO_3$ (LSMO) and AF $La_{0.7}Sr_{0.3}FeO_3$ (LSFO), and to reveal the exchange coupling mechanisms which dictate their response to an applied magnetic field.

According to a simple model based on bulk AF properties,[19] the AF spins at an ideal (111)-interface of LSFO should be fully uncompensated and they should lie in the plane of the film. However, previous results from (111)-oriented LSMO/$La_{1-x}Sr_xFeO_3$ heterostructures have shown that the orientation of the AF spin axis depends on the thickness of the $La_{1-x}Sr_xFeO_3$ layer.[20, 21] For heterostructures with thick AF layers, the AF spin axis lies within the (111) plane, while for heterostructures with relatively thin AF layers, i.e. below 18 unit cells (u.c.), the AF spin axis cants out-of-plane and can be reoriented through spin-flop coupling with the LSMO layers which in turn are reoriented by a moderate external magnetic field.[20, 22] In this work, we demonstrate our measurement protocol on two LSMO/LSFO superlattices with equal LSMO and LSFO thickness of 9 u.c. and 18 u.c. This protocol clearly shows how in some cases the AF spin axis cants out-of-plane and experiences spin-flop coupling with adjacent FM layers.

Experimental Procedure

Epitaxial LSMO/LSFO superlattices were deposited on (111)-oriented $SrTiO_3$ (STO) substrates by pulsed laser deposition. The superlattice notation is as follows: $[number\ of\ u.c.\ LSMO \times number\ of\ u.c.\ LSFO]\ number\ of\ repeats$. The LSMO layer was grown first on the STO substrate and the total thickness of the superlattices was held constant at approximately 41 nm. The $[9\times9]10$ superlattice was grown with a frequency of 5 Hz (1 Hz) and fluence of ~0.5 J cm^{-2} (~0.9 J cm^{-2}) for the growth of the LSMO (LSFO) layers. During the growth, the substrate temperature was held at 700 ℃ and the oxygen background pressure was 300 mTorr. The $[18\times18]5$ superlattice was grown with a frequency of 10 Hz and fluence of ~1.5 J cm^{-2} for both LSMO and LSFO layers with the substrate temperature held at 700 ℃ and the oxygen background pressure was 200 mTorr. The samples were cooled slowly to room temperature after the deposition with an oxygen pressure of 300 Torr to ensure proper oxygen stoichiometry. Additional samples grown under both sets of conditions exhibit the same structural and magnetic properties.

Structural characterization with high resolution x-ray diffraction and resonant x-ray reflectivity shows that the superlattices have high crystallinity with sharp interfaces without appreciable chemical intermixing, and the as-designed sublayer thicknesses.[20] The magnetic and electrical transport properties of the superlattices have been previously reported. Both the $[9\times9]10$ and $[18\times18]5$ superlattices display coincident FM-to-paramagnetic and metal-to-insulator transitions, and exchange bias is absent based on the lack of a horizontal shift of field cooled hysteresis loops.[20] Angle-dependent x-ray absorption (XA) spectroscopy measurements were performed using linearly polarized x-rays at 80 K in the vector magnet endstation [23] at beamline 4.0.2 of the Advanced Light Source using total electron yield mode. The detailed measurement geometries used are discussed below.

Results and Discussion

The Fe *L* edge XA spectra were recorded with linearly polarized x-rays at 35° grazing incidence with p- and s-polarization as a function of polar and azimuthal angles. The polar angle (θ) is defined as the angle between the x-ray ***E***-vector and the sample surface; while the azimuthal angle (ϕ) is the angle between the in-plane projection of the ***E***-vector and the $[11\bar{2}]$ direction as shown in Fig. 1(a). Within the (111) plane, the two orthogonal in-plane directions are the $[1\bar{1}0]$ and $[11\bar{2}]$ directions. Fig. 1(b) shows the measurement condition with p-polarized x-rays ($\theta = 55°$, blue curve) and s-polarized x-rays ($\theta = 0°$, red curve). Fig. 1(c) shows typical Fe L_2 edge XA spectra from the $[9\times9]10$ superlattice acquired with p-polarized x-rays ($\theta = 55°$) with $\phi = 0°$ and $180°$. A clear angular dependence can be observed as the difference in the relative peak heights of the '*a'* and '*b'* peaks of the multiplet structure. The spectral shape of the Fe XA curves correspond well to curves reported in the literature for $La_{1-x}Sr_xFeO_3$ thin films where the relative L_{2a} and L_{2b} peak intensities change with a cosine squared dependence of the angle between the AF spin axis and the x-ray ***E***-vector.[24-26]

The angular dependence of the XA spectra can be quantified by the difference in intensity between the L_{2a} and L_{2b} peaks divided by the difference between the pre-edges of the L_2 and L_3 edges.

$$L_2\ difference = \frac{L_{2a} - L_{2b}}{L_2^{pre} - L_3^{pre}}$$

Rather than using the difference or the asymmetry (i.e. difference divided by sum) values between the L_{2a} and L_{2b} peaks, the definition used here minimizes the influence from variations in incident x-ray intensities at different linear polarizations. A systematic study was carried out in three geometries chosen to probe the impact of the crystal electric field on the XA spectra as well as the response of the AF spin structure of the LSFO layers to an applied magnetic field through exchange coupling to the FM LSMO layers.

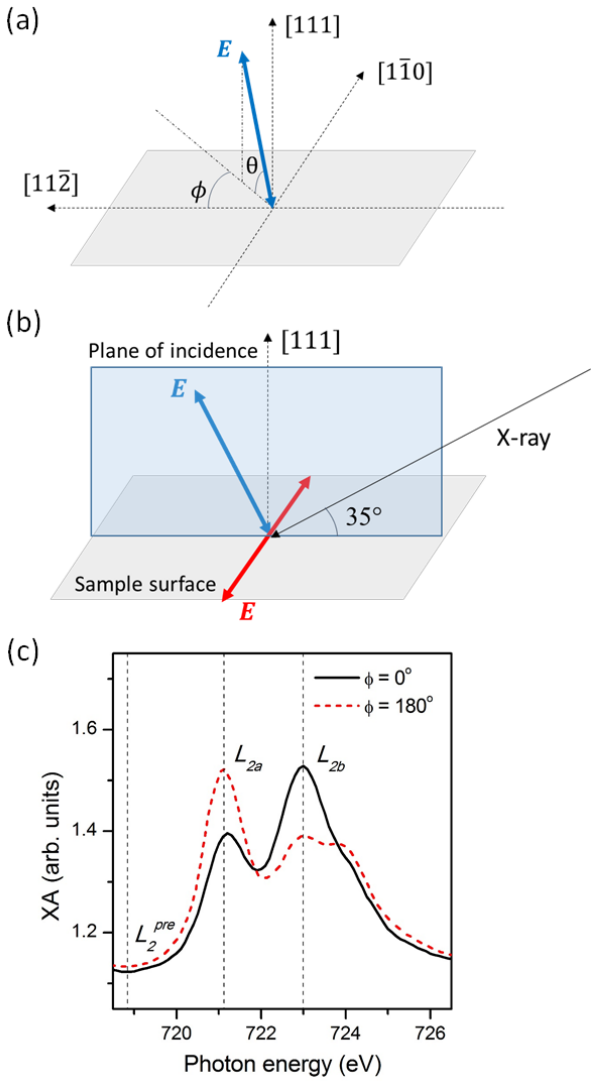

Fig. 1: (a) Definition of the polar (θ) and azimuthal (ϕ) angles; (b) Schematic of the measurement geometry with linearly polarized x-rays at 35° grazing incidence with p- (θ = 55°, blue curve) and s-polarization (θ = 0°, red curve); (c) Fe L_2 edge XA spectra taken with p-polarized x-rays for the $[9\times9]10$ superlattice at $\phi = 0°$ and $\phi = 180°$ with $\boldsymbol{H}$ parallel to the $[11\bar{2}]$ direction. Since the sample has a threefold in-plane symmetry, rather than two or fourfold symmetry, the XA spectra are expected to differ for an in-plane rotation by 180°. The L_{2a} and L_{2b} peaks and the L_2 pre-edge positions are indicated with vertical dashed lines.

According to our previous study of the $[9\times9]10$ and $[18\times18]5$ superlattices, the AF spin axis can be reoriented by a moderate applied magnetic field through spin-flop coupling with the magnetically soft LSMO sublayers.[20] However, in these studies, the exact crystallographic orientation of the AF spin axes could not be determined from the fixed geometry used. Using the angle-dependent measurements referred to as geometry 1 and shown schematically in Fig. 2(a), these crystallographic orientations which define the magnetic symmetry can be determined. In geometry 1, the x-ray polarization ***E***-vector cants out-of-plane by $\theta = 55°$ and the applied magnetic field, ***H*** = 0.3 T cants out-of-plane by $30°$. Since the easy direction of the FM layer lies in the (111) plane, ***H*** = 0.3 T is sufficient to align and fully saturate the FM moments of both superlattices in all in-plane directions. Only the in-plane component of ***H*** is shown in all schematics for simplicity. As the azimuthal angle ϕ varies, ***H*** and ***E*** are rotated together such that the angle between them is fixed and their in-plane components remain parallel. With $\theta = 55°$ and $\phi = 0°,\ 120°$, and $240°$, ***E*** lies along the $[110]$, $[101]$, and $[011]$ directions, respectively. The measurement for the $[9\times9]10$ superlattice was taken in the range from $0°$ to $120°$ and for the $[18\times18]5$ superlattice from $0°$ to $360°$.

In the scenario that the AF spin axis freely rotates with the FM moments as the azimuthal angle ϕ varies, one should see no angular dependence in the Fe L_2 difference. However, for both the $[9\times9]10$ and $[18\times18]5$ superlattices (Fig. 2(d)), a strong angular dependence is observed which can be fit by a cosine function with a period of $120°$. This period is consistent with the 3-fold rotational symmetry of the (111)-plane, and it indicates that the AF spin axes prefer to lie within a particular family of directions rather than freely rotate. Interestingly, a phase difference exists between the two samples, such that the minima of the Fe L_2 difference of the $[9\times9]10$ superlattice occur at $\phi = 0°$ and $120°$ (corresponding to the ***E***-vector lying along the out-of-plane $< 110 >$ directions), and the maximum occurs at $\phi = 60°$. In contrast, for the $[18\times18]5$ superlattice, the out-of-plane $< 110 >$ directions correspond to the *maxima* of the Fe L_2 difference instead of the minima. We attribute this difference due to a change in the preferred directions of the AF spin axes in the two superlattices given that the structural parameters and experimental geometries are the same. This phase difference demonstrates that purely crystallographic contributions to the angular dependence of the XA spectra provide a minor contribution to the overall measured signal. As shown in Fig. 2(b-c), the out-of-plane low-index crystallographic directions include the set of $[110]$, $[101]$, and $[011]$ directions which cant out-of-plane by $55°$ (corresponding to $\phi = 0,\ 120°$, and $240°$), and the set of $[100]$, $[001]$, and $[010]$ directions which cant out of plane by $35°$ (corresponding to $\phi = 60°,\ 180°$, and $300°$). Previous work by Folven *et al.* on (001)-oriented LSMO/$LaFeO_3$ (LFO) bilayers suggests that the spin axis of the LFO layer lies along the in-plane $< 100 >$ and $< 110 >$ crystalline axes. The population of the two types of domains changes with the LFO layer thickness; the domains with the AF spin axis along the $< 110 >$ directions dominate in LFO layers of 10 u.c. whereas a LFO layer of 50 u.c. shows a slightly higher proportion of domains with AF spin axis along the $< 100 >$ directions [27]. In a similar way, we infer that the spin axis of the $[9\times9]10$ superlattice with 9 u.c. thick LSFO layers lies along the $< 110 >$ directions with a spin canting angle of $55°$ to the surface and Fe L_2 difference minima at $\phi = 0°$, $120°$, and $240°$, and that of the $[18\times18]5$ superlattice with 18 u.c. thick LSFO layers lies along the $< 100 >$ directions with a canting angle of $35°$ and Fe L_2 difference minima at $\phi = 60°$, $180°$, and $300°$. It should be noted

that the minima in Fe L_2 difference correspond to the out-of-plane $< 110 >$ and $< 100 >$ crystalline axes since spin-flop coupling favors perpendicular alignment between the AF spin axis and the magnetic field. In this geometry $\boldsymbol{H}$ and $\boldsymbol{E}$ are nearly parallel to one another. Thus, the angle between a majority of the AF moments and the $\boldsymbol{E}$-vector is large (~90°) resulting in a small value for Fe L_2 difference according to the cosine squared dependence.

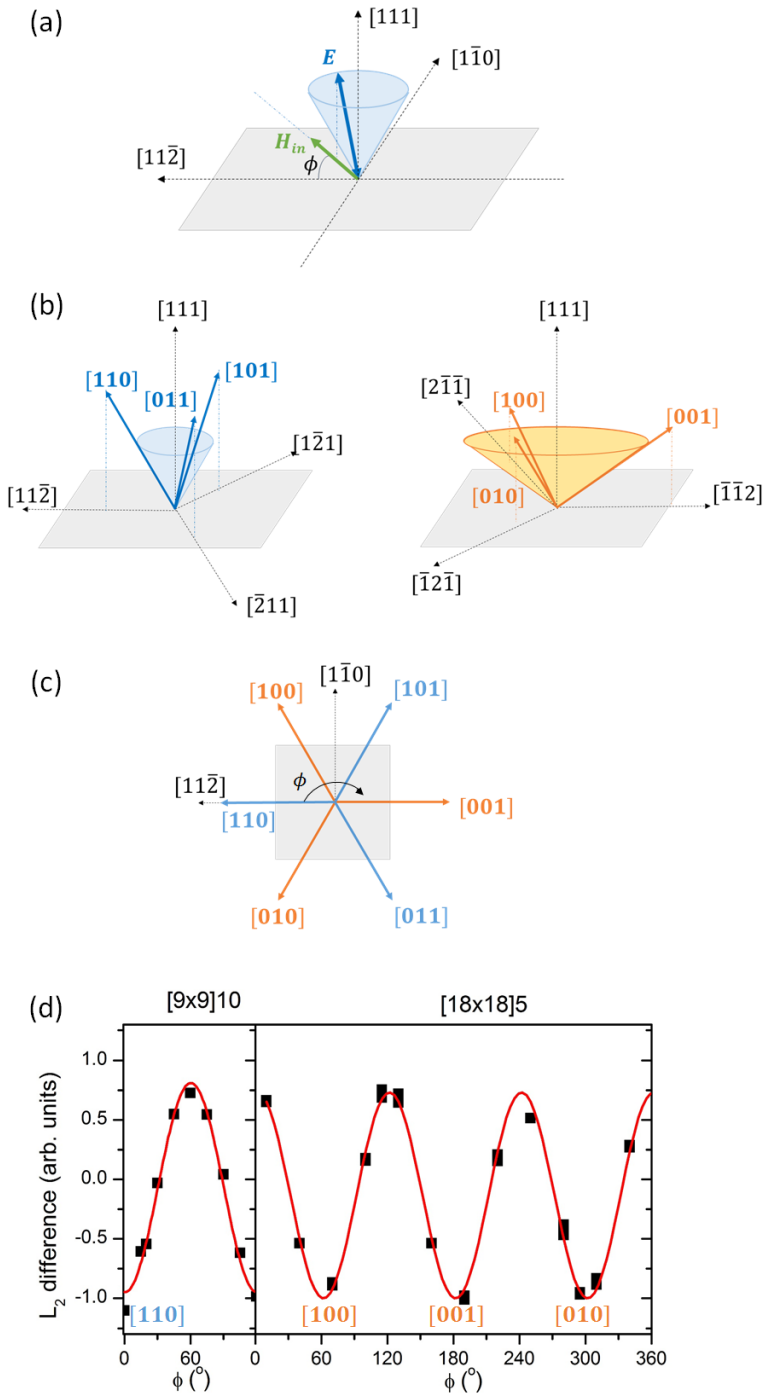

Fig. 2: (a) Schematic of measurement geometry 1 taken with p-polarized x-rays. The blue cone corresponds to a canting angle of 55°. Only the in-plane component of the applied magnetic field is shown; (b) Schematic of the out-of-plane low-index crystallographic directions; Left: [110], [101], and [011] directions with a canting angle of 55°; Right: [100], [010], and [001] directions with a canting angle of 35°; (c) The projections of the out-of-plane low-index crystallographic directions on to the (111) plane; (d) Fe L_2 difference as a function of the azimuthal angle ϕ measured in geometry 1 for the [9×9]10 and [18×18]5 superlattices. The red lines are fits to a cosine function with a period of 120°.

Now that it has been established that the AF spins prefer to align along a particular family of crystallographic directions, measurements carried out in geometry 2 (schematic shown in Fig. 3(a) and (c)) were performed to probe the relative proportion of AF domains oriented along each of the three possible variants (e.g. the [100], [010], and [001] directions for the $[18\times18]5$ superlattice). In geometry 2, the direction of $\boldsymbol{H}$ is fixed relative to the crystallographic axes while the direction of the $\boldsymbol{E}$-vector varies. $\boldsymbol{H}$ cants out-of-plane by $30°$ with the in-plane component either along the $[11\bar{2}]$ direction (geometry 2a) or the $[1\bar{1}0]$ direction (geometry 2b). For the $\boldsymbol{E}$-vector, the polar angle was kept at $\theta = 55°$ and the azimuthal angle ϕ varied from $0°$ to $360°$. Therefore, the AF spin axis remains in a fixed orientation and the "searchlight probe" of the $\boldsymbol{E}$-vector sweeps out a cone with an inner angle of 35°. Here we define ϕ_M as the angle between the in-plane component of $\boldsymbol{E}$ and the in-plane component of $\boldsymbol{H}$, such that $\phi_M = \phi$ for geometry 2a and $\phi_M = \phi - 90°$ for geometry 2b. It is worth noting that the L_2 difference in geometry 1 with $\phi = 0°$ (the in-plane component of $\boldsymbol{E}$ and $\boldsymbol{H}$ along the $[11\bar{2}]$ direction) corresponds to that in geometry 2a with $\phi_M = 0°$ and the L_2 difference in geometry 1 with $\phi = 90°$ (the in-plane component of $\boldsymbol{E}$ and $\boldsymbol{H}$ along the $[1\bar{1}0]$ direction) corresponds to that in geometry 2b with $\phi_M = 0°$. The results are consistent for both superlattices in all geometries. Unlike the angular dependence of the Fe L_2 difference obtained with geometry 1, the Fe L_2 difference of both superlattices measured in geometries 2a and 2b show a cosine dependence with a period of $360°$. The structural 3-fold symmetry is broken due to the impact of the applied magnetic field and resulting interfacial exchange coupling. For both superlattices, the angular dependence of the Fe L_2 difference measured with geometry 2b has a $90°$ phase difference relative to that measured with geometry 2a. This $90°$ phase shift arises from the combined effects of the crystal electric field and the exchange coupling with the FM layers. In the absence of crystal electric field effects, the angular dependence would be determined entirely by the relative angle between $\boldsymbol{H}$ and $\boldsymbol{E}$ (i.e. ϕ_M), yielding no difference between geometries 2a and 2b and therefore producing no phase shift. Similarly, without interfacial exchange coupling, the AF spin axis should remain aligned along a preferred family of directions regardless of the applied magnetic field. In that scenario, the Fe L_2 difference signal should retain the structural 3-fold system and should not respond to the change in the $\boldsymbol{H}$-direction for the two geometries.

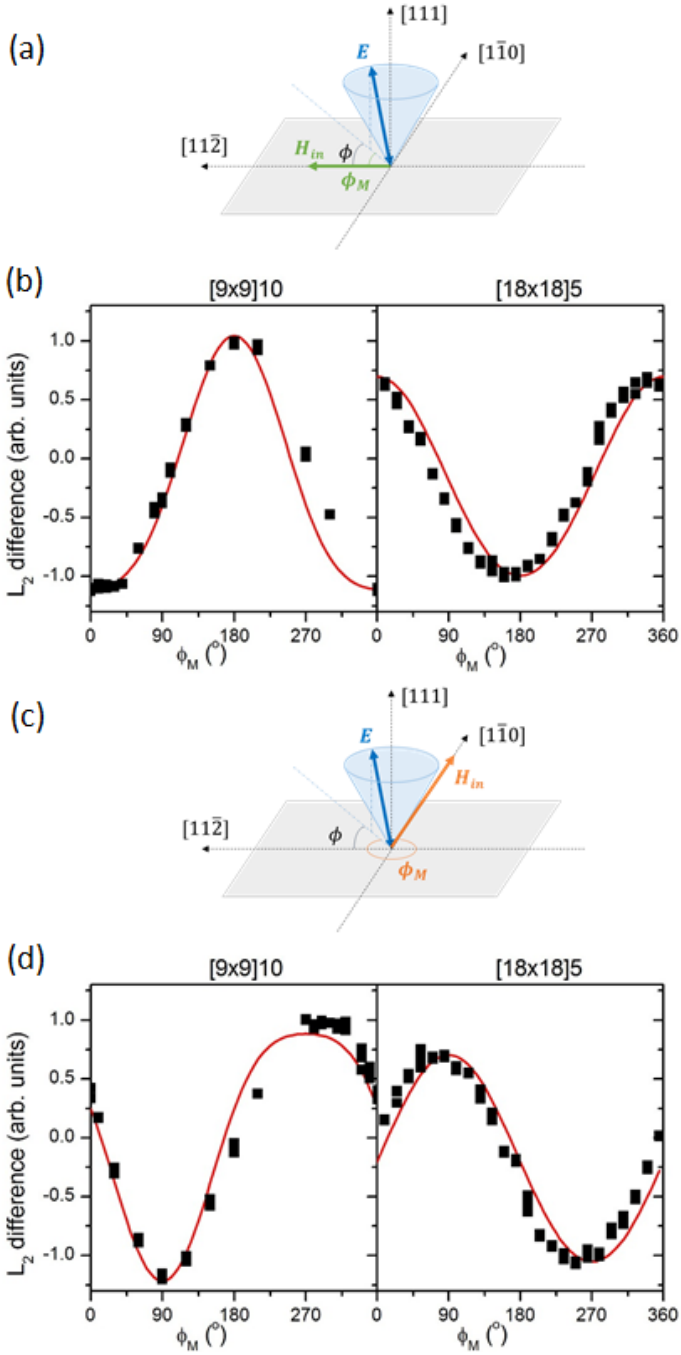

Fig. 3: (a), (c) Schematics of measurement geometries 2a and 2b performed with p-polarized x-rays. Only the in-plane component of applied magnetic field is shown; (b), (d) Fe L_2 difference as a function of the angle ϕ_M measured with geometries 2a and 2b for the $[9\times9]10$ and $[18\times18]5$ superlattices. The red lines are fits using a model described in the text.

In order to develop a full spin-model for the LSMO/LSFO system, a variant of geometry 2 was performed where the response of the in-plane component of the AF spins to exchange coupling can be probed. The in-plane component can come from both the AF domains with their spins lying fully within the (111) plane as well as the in-plane projection of the AF spins which cant out of the (111) plane. In geometry 3 (see schematics in Figure 4), the direction of $\boldsymbol{H}$ is held fixed relative to the sample with a canting angle of $30°$ and the in-plane component either along the $[11\bar{2}]$ direction (geometry 3a) or $[1\bar{1}0]$ direction (geometry 3b). In this case, the $\boldsymbol{E}$-vector lies within the (111) plane forming a circle as its direction is varied. ϕ_M and $\phi_M + 180°$ correspond to the same $\boldsymbol{E}$ direction and therefore, the Fe L_2 asymmetry of both superlattices can be fit with a cosine function with a period of $180°$. As can see in Fig. 4(b) and 4(d), two noticeable differences can be observed compared to the curves from geometry 2: no phase shift was observed between geometries 3a and 3b for both the $[9\times9]10$ and $[18\times18]5$ superlattices, and the magnitude of the Fe L_2 difference is smaller by a factor of 5 ~ 10 in geometry 3 compared to geometry 2.

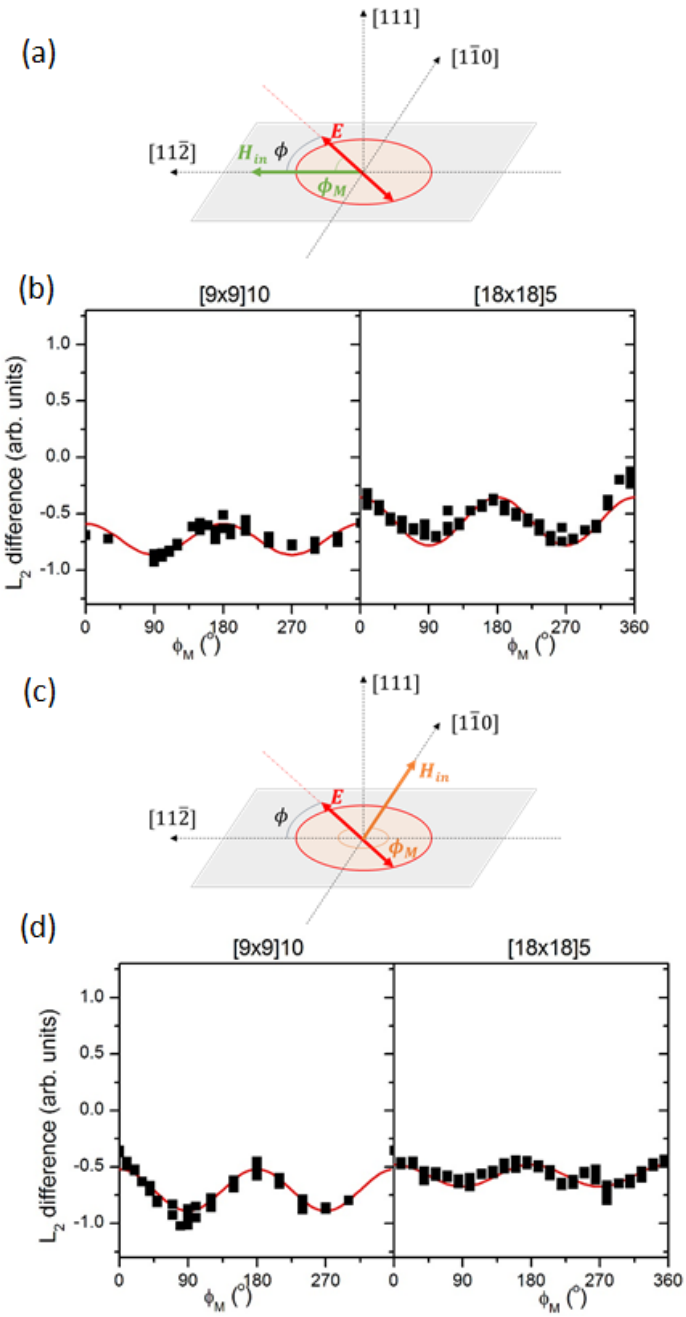

Fig. 4: (a), (c) Schematics of measurement geometries 3a and 3b performed with s-polarized x-rays. Only the in-plane component of applied magnetic field is shown; (b), (d) Fe L_2 difference as a function of the angle ϕ_M measured with geometries 3a and 3b for the $[9\times9]10$ and $[18\times18]5$ superlattices. The red lines are fits using a model described in the text.

In order to explain the angular dependence of the Fe XA spectra, we propose a model which represents a combination of the in-plane and out-of-plane AF moments for both the $[9\times9]10$ and the $[18\times18]5$ superlattices. Based on the results from geometry 1, we conclude that the out-of-plane AF moments lie along the [110], [101], and [011] directions for the $[9\times9]10$ superlattice, and the [100], [001], and [010] directions for the $[18\times18]5$ superlattice. The distribution of the AF spins into these three variants is determined by the nature of the exchange coupling relative to the magnetization direction of the FM LSMO sublayers. Assuming a spin-flop coupled interaction, the dominant out-of-plane AF spin axis lies perpendicular to (or closest to perpendicular) with the FM layer magnetization, which is a signature of spin-flop coupling [10]. For example, with geometry 2a, $\boldsymbol{H}$ cants out of the sample surface by 30° with the in-plane projection along the $[11\bar{2}]$ direction. The angle between $\boldsymbol{H}$ and the [110], [101], and [011] directions are 25°, 81°, and 81°, respectively. Thus, it is assumed that the AF spins of the $[9\times9]10$ superlattice preferentially and equally populate the AF domains with the spin axis oriented along the [101] and [011] directions, i.e. the directions that are nearly perpendicular with $\boldsymbol{H}$, and not the [110] direction which is almost parallel to $\boldsymbol{H}$.

We can calculate the angular dependence of the Fe L_2 difference arising from this spin-model using the known $cos^2\langle \boldsymbol{E}, \boldsymbol{S}\rangle$ relationship for the XMLD effect, where $\boldsymbol{S}$ is the AF spin axis [28, 29]. More specifically, the XMLD signal is modeled as $b + a_{[101]} \cdot cos^2\langle \boldsymbol{E}, \boldsymbol{S}_{[101]}\rangle + a_{[011]} \cdot cos^2\langle \boldsymbol{E}, \boldsymbol{S}_{[011]}\rangle$ where $b, a_{[101]}$ and $a_{[011]}$ are constants. With the symmetric arrangement between $\boldsymbol{H}$ and the $[101]$ and $[011]$ directions, $a_{[101]} = a_{[011]}$ and represent the relative populations of each type of domain. The parameter b accounts for the inherent difference in intensity of the A and B peaks of the multiplet structure at the Fe L_2 edge. This calculated spectra is shown in the supplemental material [30] Fig. S1(a), and displays the same cosine dependence with a period of $360°$ as observed experimentally for geometry 2 (Fig. 3). However, assuming that only the in-plane projection of these spins contribute to the signal in geometry 3a results in a curve with a 90° phase shift compared to the experimental curve (compare Fig. S1(c) to Fig. 4(b)). One possible way to resolve this difference is to assume the presence of AF domains with in-plane AF moments that are collinear with the LSMO magnetization which lies within the (111) plane [2], a configuration which can lower the exchange energy between any uncompensated AF spins and FM moments. This purely exchange biased case can be modeled as $b + a_{[11\bar{2}]} \cdot cos^2\langle \boldsymbol{E}, \boldsymbol{S}_{[11\bar{2}]}\rangle$. As shown in Fig. S2(c), this curve agrees with the shape of the experimental curve in Fig. 4(c). The final spin-model taking into account both the canted and in-plane spins can be fit to the experimental spectra with linear regression. Assuming that the [011] and [101] domains are equally populated, $a_{[011]} = a_{[101]}$, so that $a_{out} = 2a_{[011]}$ and $a_{in} = a_{[11\bar{2}]}$. From this analysis, we determine that in geometry 2a with field along the $[11\bar{2}]$ direction, 72% of the LSFO spins are found in domains where the spin axis cants out-of-plane, while the remaining 28% are found in domains with in-plane AF spin axis. The out-of-plane domains experience spin-flop coupling with the LSMO moments, while the in-plane domains are oriented parallel to the LSMO moments.

Similar analysis was performed for geometries 2b and 3b for the $[9\times9]10$ superlattice as well as both geometries for the $[18\times18]5$ superlattice. The directions of the out-of-plane and in-plane spin axes for both superlattices and all measurement geometries are listed in Tables SI and SII of the supplemental material [30], and the population of in-plane vs. out-of-plane AF moments is plotted in Fig. 5. The standard errors are extrapolated from the ratio of the expected value and standard deviation of fitting parameters of the cos^2 term. Full details on the fitting

procedure is given in the supplemental material [30] and the red lines in Fig 3(b, d) and Fig 4(b, d) are the fitting results which can reproduce the experimental angular dependence of L_2 difference quite well. With $\boldsymbol{H_{in}}$ pointing along the $[11\bar{2}]$ direction, $28 \pm 3.1\%$ of the AF moments in the $[9\times9]10$ superlattice and $26 \pm 2.5\%$ of that of the $[18\times18]5$ superlattice lie in the (111) plane. In contrast, with $\boldsymbol{H_{in}}$ pointing along the $[1\bar{1}0]$ direction, $46 \pm 2.7\%$ of the AF moments of the $[9\times9]10$ superlattice and $38 \pm 3.5\%$ of that of the $[18\times18]5$ superlattice lie in the (111) plane. The ratio between the in-plane and out-of-plane AF moments is not only dependent on the sublayer thickness of the superlattice, but is also influenced by the direction of the applied magnetic field.

The systematic analysis of the XA angular dependence carried out in three different geometries sheds light on the complicated AF structures and exchange coupling mechanisms in the (111)-oriented LSMO/LSFO superlattices. Based on the results from geometry 1, we conclude that the out-of-plane AF moments lie along the [110], [101], and [011] directions for the $[9\times9]10$ superlattice, and the [100], [001], and [010] directions for the $[18\times18]5$ superlattice. The results from geometries 2 and 3 suggest a model for the LSFO magnetic structure in which two types of AF domains exist. These domains have in-plane and out-of-plane AF spins, which are oriented parallel and perpendicular to the LSMO magnetization, respectively. The underlying reason for the complex spin model is that the energy difference between out-of-plane and in-plane states for the AF moments is small due to the symmetry of the (111)-plane. Both types of AF moments can be reoriented by an external magnetic field acting on a ferromagnet exchange coupled to the AF moments, which explains the absence of an exchange bias in the hysteresis loops of field cooled bilayer systems.[20, 31] The model is also consistent with a recent report on (111)-oriented LSMO/LFO bilayers suggesting that the different octahedra tilt patterns in the LSMO and LFO layers cause structural modifications near the interface that ultimately lead to modified magnetic orders with an induced switchable moment on the Fe^{3+} ion.[21]

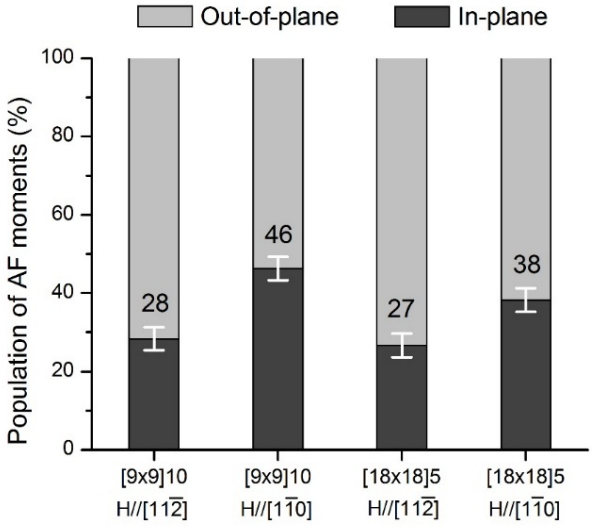

Fig. 5: Population of the in-plane *vs.* out-of-plane AF moments in the $[9\times9]10$ and $[18\times18]5$ superlattices with magnetic field applied along different in-plane directions.

Conclusion

In summary, we demonstrate the use of three measurement geometries of angle-dependent XA spectroscopy to perform a detailed study of the AF structure and exchange coupling in (111)-oriented LSMO/LSFO superlattices with different sublayer thicknesses. Using the three distinct measurement geometries, we are able to differentiate between the magnetic symmetry and the nature of the interfacial exchange interactions to the variation of XA signal without the need to perform measurements at temperatures above the Néel temperature of the antiferromagnetic layer that may not always be experimentally feasible. We find that in the ultrathin film limit, the AF spin axis does not agree with the bulk AF structure, but instead a majority of AF domains in the $[9\times9]10$ LSMO/LSFO superlattice have AF spins that cant out of the (111) plane by $55°$ such that they lie along the $[110]$, $[101]$, and $[011]$ directions. For the $[18\times18]10$ LSMO/LSFO superlattice, the majority of the AF domains have moments cants out of the (111) plane by $35°$ corresponding to the $[100]$, $[001]$, and $[010]$ directions. These out-of-plane AF domains tend to lie perpendicular to the magnetization of the FM LSMO sublayers through a spin-flop coupling interaction. In both superlattices, a minority of the AF domains have spins which lie within the (111) plane and these in-plane AF moments prefer a parallel alignment as dictated by exchange bias. Both types of AF domains can coexist due to their close energy scales, and both can be re-oriented by applying a moderate magnetic field. The complex AF structure in these (111)-oriented LSMO/LSFO superlattices illustrates that complex metal oxide heterostructures can serve as fertile ground for discovery of new magnetic phases, which may have the potential to be incorporated into next generation information technology devices based on AF materials.

Acknowledgements

This work was supported by the National Science Foundation under grant no. DMR-1411250. The Advanced Light Source, Lawrence Berkeley Laboratory, is supported by the Director, Office of Science, Office of Basic Energy Sciences of the U.S. Department of Energy (DOE) under Contract No. DEAC02-05CH11231. Part of the sample fabrication of this research was conducted at the Center for Nanophase Materials Sciences, a U.S. DOE Office of Science User Facility.

References

1. S. A. Chambers, Advanced Materials **22** (2), 219-248 (2010).
2. I. Hallsteinsen, J. E. Boschker, M. Nord, S. Lee, M. Rzchowski, P. E. Vullum, J. K. Grepstad, R. Holmestad, C. B. Eom and T. Tybell, Journal of Applied Physics **113** (18), 183512 (2013).
3. M. Gibert, P. Zubko, R. Scherwitzl, J. Íñiguez and J.-M. Triscone, Nature materials **11** (3), 195-198 (2012).
4. D. Doennig, W. E. Pickett and R. Pentcheva, Phys Rev Lett **111** (12) (2013).
5. J. Nogues, J. Sort, V. Langlais, V. Skumryev, S. Surinach, J. S. Munoz and M. D. Baro, Phys Rep **422** (3), 65-117 (2005).
6. Y.-H. Chu, L. W. Martin, M. B. Holcomb and R. Ramesh, Materials Today **10** (10), 16-23 (2007).
7. A. Bhattacharya and S. J. May, Materials Research **44** (1), 65 (2014).
8. J. Nogués and I. K. Schuller, Journal of Magnetism and Magnetic Materials **192** (2), 203-232 (1999).
9. M. Finazzi, Physical Review B **69** (6) (2004).
10. N. C. Koon, Phys Rev Lett **78** (25), 4865-4868 (1997).
11. M. Lund, W. Macedo, K. Liu, J. Nogués, I. K. Schuller and C. Leighton, Physical review B **66** (5), 054422 (2002).
12. J. W. Cai, K. Liu and C. L. Chien, Physical Review B **60** (1), 72-75 (1999).
13. W. Zhu, L. Seve, R. Sears, B. Sinkovic and S. S. P. Parkin, Phys Rev Lett **86** (23), 5389-5392 (2001).
14. E. Arenholz, G. van der Laan, R. V. Chopdekar and Y. Suzuki, Physical Review B **74** (9), 094407 (2006).
15. E. Arenholz, G. van der Laan, R. V. Chopdekar and Y. Suzuki, Phys Rev Lett **98** (19), 197201 (2007).
16. J. Wu, J. S. Park, W. Kim, E. Arenholz, M. Liberati, A. Scholl, Y. Z. Wu, C. Hwang and Z. Q. Qiu, Phys Rev Lett **104** (21), 217204 (2010).
17. G. van der Laan, E. Arenholz, R. V. Chopdekar and Y. Suzuki, Physical Review B **77** (6), 064407 (2008).
18. C. Aruta, G. Ghiringhelli, V. Bisogni, L. Braicovich, N. B. Brookes, A. Tebano and G. Balestrino, Physical Review B **80** (1), 014431 (2009).
19. U. Shimony and J. M. Knudsen, Physical Review **144** (1), 361-366 (1966).
20. Y. Jia, R. V. Chopdekar, E. Arenholz, Z. Liu, M. D. Biegalski, Z. D. Porter, A. Mehta and Y. Takamura, Physical Review B **93** (10), 104403 (2016).
21. I. Hallsteinsen, M. Moreau, A. Grutter, M. Nord, P. E. Vullum, D. A. Gilbert, T. Bolstad, J. K. Grepstad, R. Holmestad, S. M. Selbach, A. T. N'Diaye, B. J. Kirby, E. Arenholz and T. Tybell, Physical Review B **94** (20), 201115 (2016).
22. Y. Jia, R. V. Chopdekar, E. Arenholz, A. T. Young, M. A. Marcus, A. Mehta and Y. Takamura, Physical Review B **92** (9), 094407 (2015).
23. E. Arenholz and S. O. Prestemon, Review of Scientific Instruments **76** (8), 083908 (2005).
24. J. Lüning, F. Nolting, A. Scholl, H. Ohldag, J. W. Seo, J. Fompeyrine, J.-P. Locquet and J. Stöhr, Physical Review B **67** (21), 214433 (2003).
25. A. Scholl, J. Stöhr, J. Lüning, J. W. Seo, J. Fompeyrine, H. Siegwart, J.-P. Locquet, F. Nolting, S. Anders, E. E. Fullerton, M. R. Scheinfein and H. A. Padmore, Science **287** (5455), 1014-1016 (2000).
26. A. Scholl, F. Nolting, J. Stöhr, T. Regan, J. Lüning, J. W. Seo, J.-P. Locquet, J. Fompeyrine, S. Anders, H. Ohldag and H. A. Padmore, Journal of Applied Physics **89** (11), 7266-7268 (2001).

27. E. Folven, A. Scholl, A. Young, S. T. Retterer, J. E. Boschker, T. Tybell, Y. Takamura and J. K. Grepstad, Physical Review B **84** (22), 220410 (2011).
28. D. Alders, L. H. Tjeng, F. C. Voogt, T. Hibma, G. A. Sawatzky, C. T. Chen, J. Vogel, M. Sacchi and S. Iacobucci, Physical Review B **57** (18), 11623-11631 (1998).
29. J. Stöhr, A. Scholl, T. J. Regan, S. Anders, J. Lüning, M. R. Scheinfein, H. A. Padmore and R. L. White, Phys Rev Lett **83** (9), 1862-1865 (1999).
30. See Supplemental Material at [URL] for details about the model of the antiferromagnetic order, and the fitting procedure.
31. Y. Takamura, E. Folven, J. B. R. Shu, K. R. Lukes, B. Li, A. Scholl, A. T. Young, S. T. Retterer, T. Tybell and J. K. Grepstad, Phys Rev Lett **111** (10), 107201 (2013).